ARTICLE OPEN

Check for updates

Permutable SOS (symmetry operational similarity)

Sang-Wook Cheong [1 ✉], Seongjoon Lim[1], Kai Du[1] and Fei-Ting Huang[1]

Based on symmetry consideration, quasi-one-dimensional (1D) objects, relevant to numerous observables or phenomena, can be classified into eight different types. We provide various examples of each 1D type and discuss their symmetry operational similarity (SOS) relationships, which are often permutable. A number of recent experimental observations, including current-induced magnetization in polar or chiral conductors, non-linear Hall effect in polar conductors, spin-polarization of tunneling current to chiral conductors, and ferro-rotational domain imaging with linear gyration are discussed in terms of (permutable) SOS. In addition, based on (permutable) SOS, we predict a large number of new phenomena in low symmetry materials that can be experimentally verified in the future.

INTRODUCTION

The concept of SOS (symmetry operational similarity)[1,2] between specimen constituents (periodic crystallographic or magnetic lattices in an external magnetic field, electric fields or stress, and also their time evolution) and measuring probes/quantities (observables such as transmitting electrons, phonons, magnons, photons in various polarization states, including electrons or photons with spin or orbital angular momentum, bulk magnetization or polarization, and also experimental setups to measure, e.g., Hall-type effects) in relation to broken symmetries is powerful to understand and predict observable physical phenomena in low symmetry materials[3]. Precisely speaking, this SOS relationship means that specimen constituents have identical or more (but not less) broken symmetries, compared with measuring probes/quantities. In other words, in order to have an SOS relationship, specimen constituents cannot have higher symmetries than measuring probes/quantities do. The power of the SOS approach lies in providing readily understandable views of otherwise complex and unintuitive phenomena in low-symmetry materials.

In conjunction with the earlier publications, we here discuss (quasi-)one-dimensional objects (simply referred to as 1D objects): objects can be specimen constituents (periodic lattices in the presence of external perturbations) or measuring probes/quantities (observables), and (quasi-)1D refers objects that have a certain rotation symmetry around the 1D direction, and all rotational symmetry, possibly except C_2 symmetry, is broken around any directions perpendicular to the 1D direction. Note that periodic crystallographic or magnetic lattices can have two, three, four, or sixfold rotational symmetries (C_2, C_3, C_4, or C_6 symmetries in the standard crystallographic notations, respectively), 1D specimen constituents must have at least, C_2 or C_3 symmetry around the 1D direction, and broken all of C_3, C_4, and C_6 symmetries around any directions perpendicular to the 1D direction. One example of 1D objects is cycloidal spins having SOS with polarization (P), and cycloidal spins do have C_2 symmetry around P, but no rotation symmetry, including C_2, around any direction perpendicular to the P direction[1].

Herein, we use these symmetry operation notations: **R** = twofold rotation with the rotation axis perpendicular to the 1D object direction, **R** = twofold rotation with the rotation axis along the 1D object direction, **I** = space inversion, **M** = mirror reflection

with the mirror perpendicular to the 1D object direction, **M** = mirror reflection with the mirror plane containing the 1D object direction, **T** = time reversal. In the standard crystallographic notations, "**R**, **R**, **I**, **M**, **M**, and **T**" are $C_{2\perp}$, $C_{2\parallel}$, $\bar{1}$, $m_\perp$, $m_\parallel$, $1'$, respectively[1]. Our notations are natural and intuitive to consider 1D objects. Emphasize that since we consider 1D objects, translational as well as rotational symmetry operations along the 1D object direction are freely allowed[1]. For example, **T** symmetry in a simple 1D antiferromagnet is considered to be not broken since translation is freely allowed. In addition, if the symmetry is preserved after a symmetry operation followed by a rotation around the 1D object direction, then we say that the symmetry is not broken.

Hlinka has proposed that there exist eight kinds of vectorlike physical quantities in terms of their invariance under spatiotemporal symmetry operations[4]. In fact, our 1D objects are similar to the vectorlike physical quantities in terms of symmetry, so there are eight kinds of 1D objects. We will call them as $\mathscr{D}, \mathscr{C}, \mathscr{P}, \mathscr{A}, \mathscr{D}', \mathscr{C}', \mathscr{P}', \mathscr{A}'$. Here $\mathscr{D}, \mathscr{C}, \mathscr{P}$, and $\mathscr{A}$ refer to the director, chirality, polarization, and rotational axial (electric toroidal) vector, respectively, and $'$ refers to the time-reversal broken version. All left-hand-side 1D objects ($\mathscr{D}, \mathscr{C}, \mathscr{D}', \mathscr{C}'$) in Fig. 1 have not-broken **R** (i.e., they are director-like) and all right-hand-side 1D objects ($\mathscr{P}, \mathscr{R}, \mathscr{P}', \mathscr{R}'$) have broken **R** (i.e., they are vector-like).

RESULTS AND DISCUSSION

Eight types of 1D objects

We have attempted to identify various exemplary 1D objects that show SOS with each of the eight Hlinka's classifications[4], which are listed in Fig. 1 and described below:

$\mathscr{D}$ (no broken symmetry): director. Simple antiferromagnetic order in a chain, up-up-down-down antiferromagnetic order in a chain, and up-up-down-down antiferromagnetic order in a chain with two kinds of bonding. For example, the magnetic point group $mmm1'$ (#8.2.25) has **I**, **R**, **R**, **M**, **M**, **T**, so fit the criteria for $\mathscr{D}$.

$\mathscr{C}$ (broken {**I**, **M**, **M**}): chirality. Crystallographic chirality, helical spins, a magnetic toroidal moment with the out-of-plane canted moment, a magnetic quadrupole moment with alternating out-of-plane canted moments, linear momentum (velocity) with spin or

[1]Department of Physics and Astronomy, Rutgers Center for Emergent Materials, Piscataway, NJ, USA. ✉email: sangc@physics.rutgers.edu
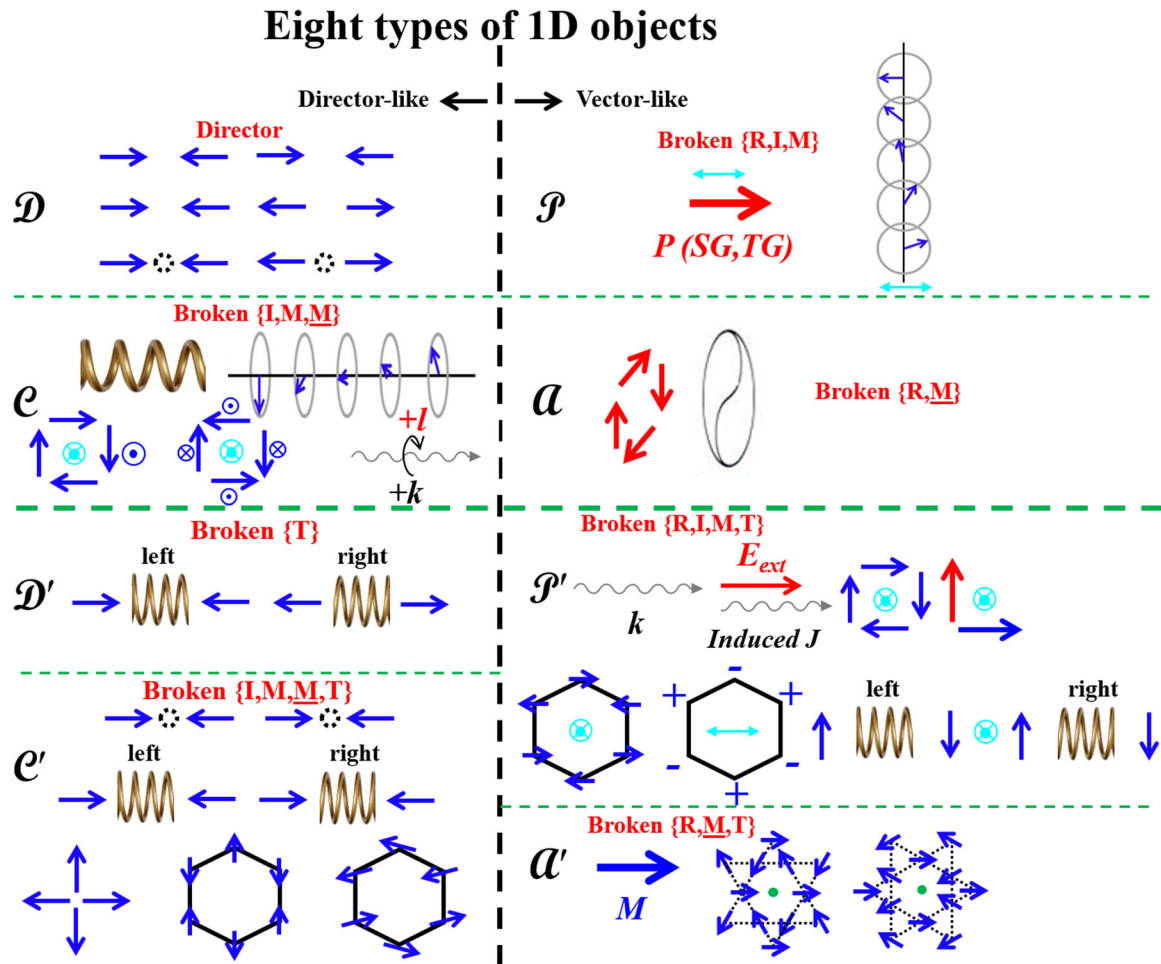
Eight types of 1D objects

Fig. 1 Eight types of 1D objects. Each type has a particular set of broken symmetries: $\mathscr{D}$; no broken symmetry, $\mathscr{C}$; broken {I, M, $\underline{M}$}, $\mathscr{D}'$; broken {T}, $\mathscr{C}'$; broken {I, M, $\underline{M}$, T}, $\mathscr{P}$; broken {R, I, M}, $\mathscr{a}$; broken {R, $\underline{M}$}, $\mathscr{P}'$; broken {R, I, M, T}, $\mathscr{a}'$; broken {R, $\underline{M}$, T}. When {T} is additionally broken, then $\mathscr{D}$, $\mathscr{C}$, $\mathscr{P}$, and $\overline{\mathscr{a}}$ become $\mathscr{D}'$, $\mathscr{C}'$, $\mathscr{P}'$, $\mathscr{a}'$, respectively. Note that all left-hand-side 1D objects ($\mathscr{D}$, $\mathscr{C}$, $\mathscr{D}'$, $\mathscr{C}'$) have not-broken {R}, so they are director-like, and all right-hand-side 1D objects ($\mathscr{P}$, $\mathscr{R}$, $\mathscr{P}'$, $\mathscr{R}'$) have broken {R}, so they are vector-like. A large number of quasi-1D schematic examples are also shown: blue arrows are spins or magnetization, red arrows are polarizations or electric fields, wiggly arrows are velocity vectors or linear momenta, "$+l$" represents angular momentum or circular polarization, light-blue symbols depict the reference 1D direction, green dots are inversion centers, dashed black circles are anions, and golden springs represent mono-axial chiral objects. The reference 1D direction is the horizontal direction on the page plane, except when there is an explicit light-blue symbol depicting the 1D direction.

orbital angular momentum along the linear momentum direction, circularly-polarized light, and vortex beam having orbital angular momentum along the vortex beam direction. For example, the point groups 222, 32, 422, 622, and 23 fit the criteria of broken {I, M, $\underline{M}$}.

$\mathscr{P}$ $\overline{(\text{broken } \{R, I, M\})}$: polarization ($P$). Strain gradient, thermal gradient, and cycloidal spins. For example, the point groups 2mm, 3m, 4mm, and 6mm fit the criteria of broken {R, I, M}.

$\mathscr{a}$ (broken {R, $\underline{M}$}): axial vector of ferro-rotation. Crystallographic rotational distortions, and electric toroidal moment. For example, the point groups $\overline{1}, \overline{3}, \overline{4}, \overline{6}$, 2/m, 4/m, and 6/m fit the criteria of broken {R, $\underline{M}$}.

$\mathscr{D}'$ (broken {T}): a director with broken {T}. Up-up-down-down antiferromagnetic order in a chain with alternating two kinds of chiral bonding environments. For example, the magnetic point group mmm (#8.1.24) has I, R, $\underline{R}$, M, $\underline{M}$, so fit the criteria for $\mathscr{D}'$.

$\mathscr{C}'$ (broken {I, M, $\underline{M}$, T}): chirality with broken {T}. Simple antiferromagnetic order in a chain with two kinds of bonding, simple antiferromagnetic order in a chain with alternating two kinds of chiral bonding environments, which corresponds to the magnetic state of Cr_2O_3, magnetic monopole, an in-plane antiferromagnetic order on the honeycomb lattice, and an

in-plane antiferromagnetic order with in-plane canting on the honeycomb lattice. For example, the magnetic point groups $\overline{3}'$m' (#20.4.74) and 6m'm' (#25.4.94) fit the criteria of broken {I, M, $\underline{M}$, T}.

$\mathscr{P}'$ (broken {R, I, M, T}): velocity (k, linear momentum, wave vector). The act of applying electric field inducing electric current, magnetic toroidal moments, an in-plane antiferromagnetic order on a honeycomb lattice, Ising antiferromagnetic order on a honeycomb lattice, and antiferromagnetic order in a chain with alternating two kinds of chiral bonding environments, corresponding to the spin-flopped state of Cr_2O_3. Note that all specimen constituents with the $\mathscr{P}'$ character can exhibit non-reciprocal directional dichroism. For example, the magnetic point group 6mm1' (#25.2.92) fits the criteria of broken {R, I, M, T}.

$\mathscr{a}'$ (broken {R, $\underline{M}$, T}): axial-vector with broken {T}. Magnetization (M), and two kinds of magnetic order in kagome lattice having SOS with M. For example, the magnetic point groups $\overline{3}$m' (#20.5.75) fits the criteria of broken {R, $\underline{M}$, T}. The magnetic point groups 2'/m' (5.5.16) and $\overline{1}$ (#2.1.3), which correspond to the magnetic states of α-Fe_2O_3 above and below the Morin transition, respectively, have broken {R, $\underline{R}$, M, $\underline{M}$, T}, so does have SOS with $\mathscr{a}'$.
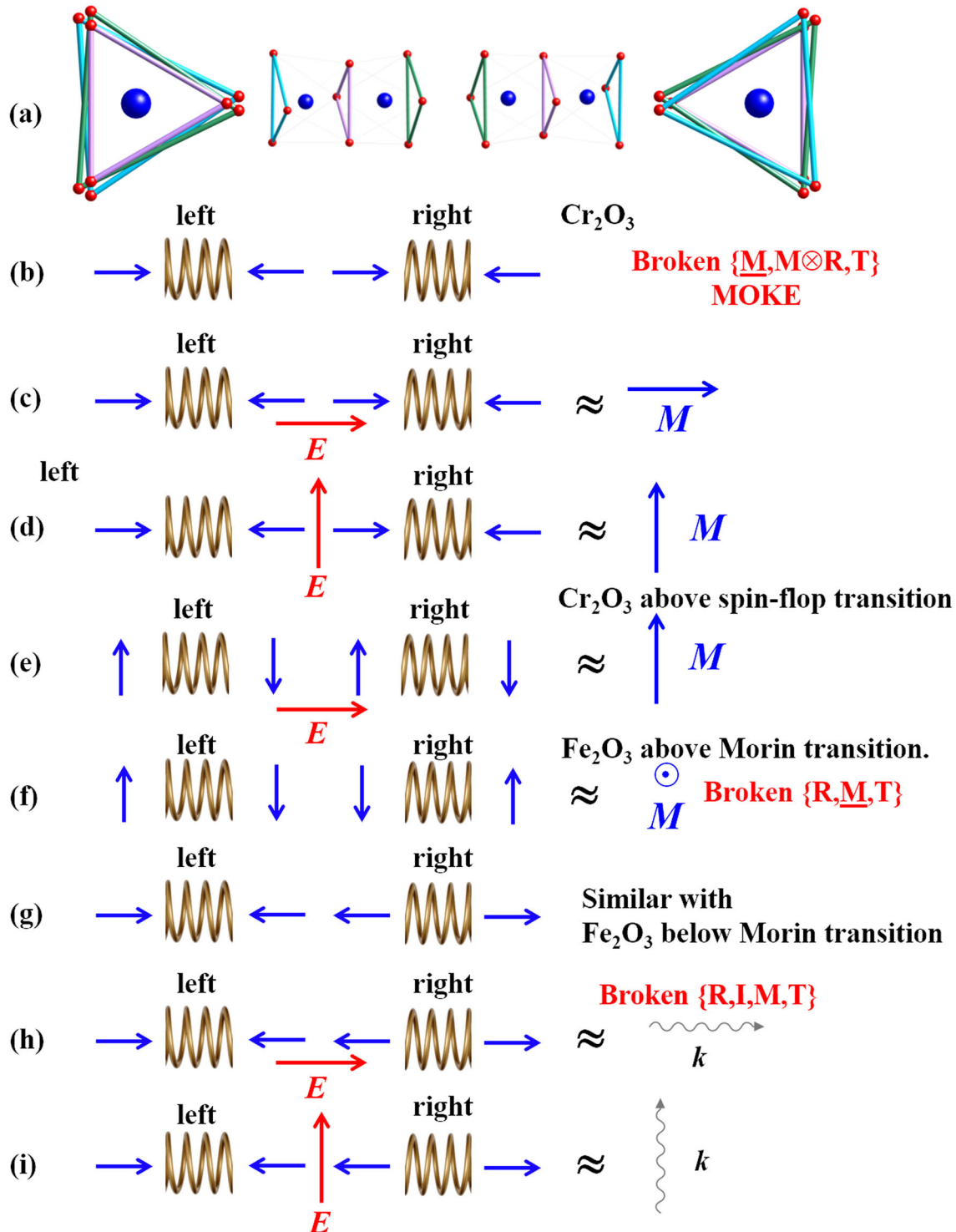
Fig. 2 Various magnetic states of Cr₂O₃ or α-Fe₂O₃, and their SOS relationships. a Crystallographic structure of a *c*-direction chain of Cr₂O₃ or α-Fe₂O₃, and left-chiral and right-chiral arrangements of three oxygen tringles are shown in the left-hand-side and right-hand-side projections along the c axis, respectively. **b** The magnetic state of Cr₂O₃ with broken {M, M⊗R, T}, so can exhibit MOKE. **c, d** The magnetic state of Cr₂O₃ in **E** shows SOS with **M**. **e** The spin-flopped state of Cr₂O₃ in **E** shows SOS with **M**. **f** The magnetic state of α-Fe₂O₃ above the Morin transition has SOS with **M**. **g** This magnetic state has no SOS with any **M**, and is somewhat similar with the magnetic state of α-Fe₂O₃ below the Morin transition. However, the magnetic state of α-Fe₂O₃ below the Morin transition has lower symmetries ($\bar{1}$), and turns out to have SOS with **M** in any arbitrary direction. **h, i** The magnetic state of α-Fe₂O₃ below the Morin transition in **E** has SOS with **k**.

As exemplary cases, we, first, discuss how our SOS approach can be helpful to understand the physics of Cr₂O₃ with linear magnetoelectricity and α-Fe₂O₃ with a canted magnetic moment and also to predict a new phenomenon in α-Fe₂O₃. In both Cr₂O₃ and α-Fe₂O₃, the 3D lattice consists of a simple hexagonal stacking of 1D *c*-direction chains of magnetic ions with alternating left-right chiral bonding environments, as shown in Fig. 2a. Magnetic orders in Cr₂O₃ and α-Fe₂O₃ above the Morin transition are schematically
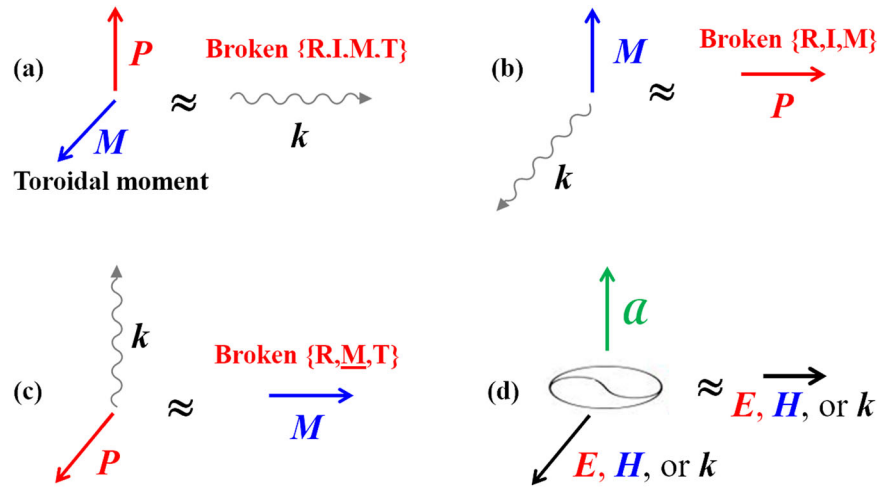
Fig. 3 Three permutable SOS among $\mathscr{a}'$, $\mathscr{P}$, and $\mathscr{P}'$ and SOS relationships with $\mathscr{a}$. Magnetization (M or magnetic field H), polarization (P or electric field E), and velocity (k) are representative for $\mathscr{a}'$, $\mathscr{P}$, and $\mathscr{P}'$, respectively. **a** $P \times M$ has broken {R, I, M, T} along the horizontal direction in the page plane, so has SOS with k. **b** $M \times k$ has broken {R, I, M} along the horizontal direction, so has SOS with P. **c** $k \times P$ has broken {R, $\underline{M}$, T} along the horizontal direction, so has SOS with M. **d** $E \times \mathscr{a}$ has broken {R, I, M} along the horizontal direction, so has SOS with P, $H \times \mathscr{a}$ has broken {R, M, T} along the horizontal direction, so has SOS with M, and $k \times \mathscr{a}$ has broken {R, I, M, T} along the horizontal direction, so has SOS with $\overline{k}$.

shown in Fig. 2b, f, respectively, so they correspond to $\mathscr{C}'$ and $\mathscr{a}'$, respectively. In the case of Cr_2O_3, the magnetic state in Fig. 2b has broken {I, M, $\underline{M}$, T}, and we can construct an SOS relationship by adding further broken symmetries such as broken {R, I, M} of P or electric field E. As shown in Fig. 2c, d, the magnetic state of Cr_2O_3 in the presence of an electric field does have SOS with M, so it shows a diagonal linear magnetoelectric effect[5]. Applying a large magnetic field along the c axis induces a spin-flopped state, shown in Fig. 2e, and this state exhibits an off-diagonal linear magnetoelectric effect, as the SOS in Fig. 2e indicates. The canted magnetic state of α-Fe_2O_3 above the Morin transition is consistent with the SOS in Fig. 2f. The magnetic state in Fig. 2g has no SOS with any M, and is somewhat similar with the magnetic state of α-Fe_2O_3 below the Morin transition. However, the magnetic state of α-Fe_2O_3 below the Morin transition has lower symmetries ($\overline{1}$), and turns out to have SOS with M in any arbitrary direction. Note that the schematic in Fig. 2b has broken {$\underline{M}$, $M \otimes R$, T}, so is supposed to exhibit a magnetooptical Kerr effect (MOKE), and indeed, does show non-zero MOKE in Cr_2O_3[2,6]. It is very interesting to notice that the magnetic state of α-Fe_2O_3 below the Morin transition in the presence of an electric field does show SOS with k, which means that it can exhibit a non-reciprocal effect such as an optical-diode effect, which can be experimentally confirmed in the future.

We emphasize that $\mathscr{D}$, $\mathscr{C}$, $\mathscr{P}$, $\mathscr{a}$, $\mathscr{D}'$, $\mathscr{C}'$, $\mathscr{P}'$, and $\mathscr{a}'$ are well-defined and all distinct, and when a specimen constituent has SOS with one of ($\mathscr{D}$, $\mathscr{C}$, $\mathscr{P}$, $\mathscr{a}$, $\mathscr{D}'$, $\mathscr{C}'$, $\mathscr{P}'$, $\mathscr{a}'$), the specimen constituent can have more (but not less) broken symmetries than the one. We also note that, for example, broken {R, $\underline{M}$, T} for M (or $\mathscr{a}'$) lists all "independently broken" symmetries, so, I is not broken and consequently I$\otimes$T is broken for M (or $\mathscr{a}'$). Thus, I is not broken in M (or $\mathscr{a}'$), but some real 3D ferromagnets, having SOS with M (or $\mathscr{a}'$), can have broken I. However, no ferromagnets can have higher symmetries than M (or $\mathscr{a}'$). Thus, all ferromagnets do have also broken I$\otimes$T since I$\otimes$T is broken in M (or $\mathscr{a}'$). In other words, real 3D ferromagnets can have all broken I, T, and I$\otimes$T. Thus, the necessary and sufficient condition for ferromagnetism or a non-zero net magnetic moment in real 3D materials is having SOS with M (or $\mathscr{a}'$) having broken {R, $\underline{M}$, T}.

Permutable SOS of $\mathscr{P} \times \mathscr{P}' \approx \mathscr{a}'$

The usefulness of the SOS approach is that it can be commonly applied to various physical quantities that share the same set of broken symmetries. $\mathscr{P}$ can be polarization (P) or an electric field (E), but it can be also a temperature gradient, strain gradient, or surface effective electric field, $\mathscr{P}'$ can be velocity/wave vector (k) of electric current, spin-wave or thermal current, or toroidal moment, and $\mathscr{a}'$ is magnetization (M) or magnetic field (H). Moreover, the SOS relationships established among them can sometimes be permutable. Figure 3a–c shows pictorially the permutable SOS relationships of $\mathscr{P} \times \mathscr{a}' \approx \mathscr{P}'$, $\mathscr{a}' \times \mathscr{P}' \approx \mathscr{P}$, $\mathscr{P}' \times \mathscr{P} \approx \mathscr{a}'$, respectively. Note that all of $\mathscr{P}$, $\mathscr{P}'$, and $\mathscr{a}'$ are vector-like, i.e., not director-like.

It turns out that the motion of quasiparticles such as electrons, phonons, magnons, and photons in a specimen or the motion of the specimen itself can be non-reciprocal if the specimen constituent has SOS with k of the motion. If a symmetry operation links $+k$ and $-k$, and a specimen constituent where quasiparticles are moving with $\pm k$ is invariant under the symmetry operation, then the experiment becomes reciprocal, i.e., there is no difference between the experimental results with $+k$ and those with $-k$. On the other hand, when a specimen constituent has SOS with k, then there is no symmetry operation that can link these two experiments: a specimen constituent with $+k$ and the identical specimen with $-k$. Thus, the experiments can be non-reciprocal. Note that the magnitude of non-reciprocal effects cannot be estimated from symmetry considerations alone, and this estimation requires an understanding of the microscopic mechanism of the non-reciprocal effects. Thus, Fig. 3a means that if H is applied to any polar magnets, then the electron, light, phonons, or spin-wave propagation can be non-reciprocal, i.e., exhibit directional dichroism. Indeed, for example, diode-like light propagation has been observed in polar $(Fe, Zn)_2Mo_3O_8$ in H[7], and electron transport in polar BiTeBr[8] in H turns out to be non-reciprocal in experimental configurations consistent with Fig. 3a. We anticipate that applying in-plane H to polar $Fe(Mn, Ni, Zn)_2Mo_3O_8$ or polar (and chiral) Ni_3TeO_6[9] will induce a non-reciprocal spin-wave along the in-plane direction perpendicular to H.

Figure 3b represents all kinds of (anomalous) Hall-type effects (Hall, Ettingshausen, Nernst, and thermal Hall). Here, (k and P) represents (electric current and induced voltage), (electric current and induced thermal gradient), (thermal gradient and induced

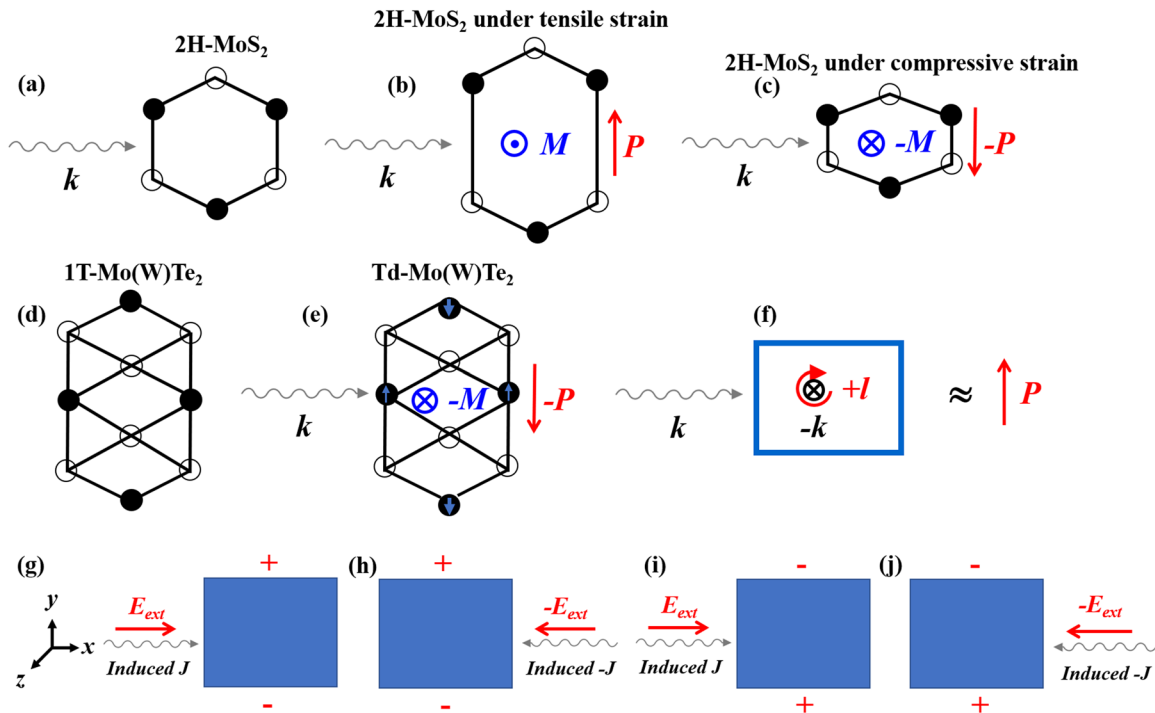**Fig. 4 Current-induced _M_, circular dichroism Hall effect (CDHE), and non-linear Hall effect (NLHE). a–c** Monolayer of 2H-MoS$_2$: (**a**); no strain, (**b**); uni-directional uniform tensile strain along the vertical direction on the page plane, and (**c**); uni-directional uniform compressive strain along the vertical direction on the page plane. **d, e** show monolayer 1T-Mo(W)Te$_2$ and T$_d$-Mo(W)Te$_2$, respectively. Closed black circles, dark-blue arrows, open black circles, wiggly arrows, red arrows, and blue symbols represent cations, cation distortions, anions, uniform electric currents, polarizations, and induced magnetizations, respectively. Thus, (**b**), (**c**), and (**e**) represent the current-induced magnetization in polar conductors. This current-induced magnetization is directly related to the presence of non-linear Hall effects in polar conductors without any external magnetic field. **f** depicts the SOS relationship for CDHE with the electric current flow with _k_, circular-light illumination with $-k$ and $+l$, and _P_ representing the induced Hall voltage. **g–j** Four possible configurations of Hall-type voltages induced by electric currents in external electric fields.

voltage), and (thermal gradient and induced thermal gradient) for the Hall, Ettingshausen, Nernst, and thermal Hall effects, respectively. Figure 3c can also represent numerous physical phenomena, including the off-diagonal linear magnetoelectric effect in Cr$_2$O$_3$ in the spin-flopped state (Fig. 2e), the spin Hall effect, the spin Nernst (or thermal spin Hall) effect, current-induced magnetization in polar conductors, and also non-linear Hall effects in polar conductors[10]. Note that $\mathscr{A}' \times \mathscr{P}' \approx \mathscr{P}$ and $\mathscr{P}' \times \mathscr{P} \approx \mathscr{A}'$ indicate that all magnetic states having SOS with $\mathscr{P}'$ should exhibit off-diagonal linear magnetoelectric effects. When _P_ represents the surface effective electric field, electric current and thermal current for _k_ can induce spin current flow along the direction perpendicular to _P_ and the current direction—the resulting surface magnetization is represented by _M_. Here, the electric current and the thermal current correspond to the spin Hall effect and the spin Nernst (or thermal spin Hall) effect, respectively. Figure 3c also represents that electric current, thermal current, or light propagation along a direction perpendicular to _P_ in polar materials can induce _M_ along the direction perpendicular to both the _P_ and the current/light propagation directions. Even though _M_ in polar materials induced by thermal current/light has not been reported, _M_ in polar conductors induced by electric current has been reported, interestingly in an exotic material of strained monolayer MoS$_2$[11,12]. It will be interesting to observe this current-induced _M_ in bulk non-magnetic polar conductors such as Ca$_3$Ru$_2$O$_7$, GeTe, TaAs, and BiTeI(Br, Cl)[13–16]. In addition, it will be fundamentally important to observe _M_ in polar materials induced by thermal current or light—in this case, the polar materials do not have to be electric conductors, in principle.

The monolayer of 2H-MoS$_2$, shown in Fig. 4a, is non-centrosymmetric, but non-polar due to the presence of C$_3$ symmetry. However, uniaxial uniform strain along a particular in-plane direction breaks the C$_3$ symmetry and induces _P_ in the direction perpendicular to the strain. When an electric current is applied to an in-plane direction perpendicular to the strain-induced _P_, then _M_ develops along the out-of-plane direction, which is depicted in Fig. 4b, c. Tensile and compressive strains result in opposite _M_s. A similar situation, but without external strain, should also work for monolayer T$_d$-WTe$_2$ or T$_d$-MoTe$_2$. Monolayer T$_d$-WTe$_2$ or T$_d$-MoTe$_2$ with W/Mo zigzags does have in-plane polarization perpendicular to the zigzag direction. When an electric current is applied along the zigzag direction, _M_ along the out-of-plane direction should be induced, which requires future experimental confirmation. In fact, this _M_ induced by electric current in polar conductors is directly related to the presence of the non-linear Hall effect that we will discuss next.

First, we attempt to figure out the requirement for quadratic-type non-linear Hall effect (NLHE) without any applied magnetic field. We consider four Fig. 4g–j situations of Hall-type voltages with an applied external electric field ($+ -E_{ext}$). To discuss the 3D arrangements of NLHE measurements, we will use these notations: R_x = twofold rotation operation around the _x_-axis, M_x = mirror operation with the mirror perpendicular to the _x_-axis, etc. Any of {R_y, M_x, M_z, **T**} links between Fig. 4g, h (or, (g) or (h) itself). NLHE should not depend on the sign of the external _E_, so NLHE may require not-broken {R_y, M_x, M_z, **T**}. However, breaking any of {R_y, M_x, M_z, **T**} does not make NLHE vanish. Now, any cross-link between Fig. 4g/h, i/j can happen with {R_x, R_z, **I**, M_y}, so not-broken any of {R_x, R_z, **I**, M_y} will lead to NLHE to vanish. Therefore, broken {R_x, R_z, **I**, M_y} is required to have non-zero NLHE. {R_x, R_z, **I**, M_y}

becomes {**R**, **I**, **M**} with the respect to the vertical reference direction on the page plane (i.e., the y-axis). Thus, broken {**R**, **I**, **M**}, more precisely speaking broken {$\mathbf{R_x}$, $\mathbf{R_z}$, **I**, $\mathbf{M_y}$}, is the necessary and sufficient condition for non-zero NLHE. **P** has broken {**R**, **I**, **M**} and also not-broken {$\mathbf{R_y}$, $\mathbf{M_x}$, $\mathbf{M_z}$, **T**}, but in principle, any specimen constituents having SOS with **P** can exhibit non-zero NLHE. In other words, the specimen constituents with non-zero NLHE can have lower symmetry than **P** (i.e., can have broken some of {$\mathbf{R_y}$, $\mathbf{M_x}$, $\mathbf{M_z}$, **T**}). Note that in principle, broken {$\mathbf{R_x}$, $\mathbf{R_z}$, **I**, $\mathbf{M_y}$} can be achieved in any of non-centrosymmetric materials when the x, y, and z axes are properly chosen, even though the magnitudes of NLHE maybe not significant when the x, y, and z axes are not along with the principal crystallographic directions.

Now, there exists a straightforward but elegant relationship between current-induced magnetization and NLHE in polar conductors. When an electric current, **J**, is applied to a polar conductor along a direction perpendicular to **P**, **M** is induced along a direction perpendicular to both **J** and **P**. This, induced **M** acts like a magnetic field for the standard Hall effect, and Hall voltage along the **P** direction goes like $\mathbf{J} \times \mathbf{M} \propto \mathbf{J}^2$, which explains quadratic-type non-linear Hall effect in polar conductors. Therefore, strained monolayer MoS_2 should exhibit NLHE along the strain-induced **P** direction. In fact, the observation of NLHE in ultrathin WTe_2 may be consistent with the above discussion[17]. Note that bulk non-magnetic polar conductors such as $Ca_3Ru_2O_7$, GeTe, TaAs, and BiTeI(Br, Cl) should exhibit NLHE, in addition to current-induced **M**.

We also note that the so-called circular dichroism Hall effect can be understood on a similar footing[18]. Illumination of circularly-polarized light on a chiral material can induce an electric current, which is called a circular photogalvanic effect (CPGE)[19–21]. In the case of CPGE, one can consider if or not the entire experimental setup with induced current changes in a systematic manner under all symmetry operations—the so-called symmetry operational systematics (SOSs). It turns out that in terms of SOSs, a similar phenomenon can occur in a material with a net magnetic moment, rather than chirality[1]. Now, with the consideration of SOSs, one can also show that illumination of circularly-polarized light on any materials can induce **M**. This circularly-polarized light-induced **M** can act as a magnetic field, so when electric current flows along a direction perpendicular to the induced **M**, then a Hall voltage can develop along the direction perpendicular to both **M** and current without any applied magnetic field, which is called a circular dichroism Hall effect (CDHE). Therefore, in principle, this CDHE can occur in any materials where electric current flow is possible. This CDHE can be also understood in terms of the SOS relationship in Fig. 4f. Emphasize that the specimen showing with a blue rectangle appears to have no broken symmetries, but the SOS relationship still holds even if the specimen has any broken symmetries by the definition of an SOS relationship. This again guarantees that CDHE can occur in any materials where electric current flow is possible. In addition, the electric current flow can be replaced by the thermal current, and also **P** can stand for a thermal gradient, rather than a Hall voltage. Therefore, there can exist Ettingshausen, Nernst, or thermal Hall effect versions of CDHE in any materials with circularly-polarized light (or vortex beam with orbital angular momentum) illumination without any applied magnetic field.

We would like to discuss three more cross-product-type SOS relationships: $\mathscr{P} \times \boldsymbol{\alpha} \approx \mathscr{P}$, $\boldsymbol{\alpha}' \times \boldsymbol{\alpha} \approx \boldsymbol{\alpha}'$, and $\mathscr{P}' \times \boldsymbol{\alpha} \approx \mathscr{P}'$, which are illustrated in Fig. 3d. Note that all of $\mathscr{P}$, $\boldsymbol{\alpha}$, $\mathscr{P}'$, and $\boldsymbol{\alpha}'$ are vector-like (thus, not director-like). The meaning of these SOS relationships is: when an electric field or a magnetic field is applied to a ferro-rotational system, the induced polarization or magnetization can have a component along the direction perpendicular to the applied **E/H** and also to the $\boldsymbol{\alpha}$ direction. In other words, in ferro-rotational systems in the presence of an external electric field or magnetic field, the induced polarization or magnetization can

be tilted toward the direction perpendicular to the applied **E/H** and also to the $\boldsymbol{\alpha}$ direction. The tiled induced polarization can be a tilted current in ferro-rotational conductors, so a Hall-type voltage can develop without any external magnetic field. As far as we are aware of, any observations relevant to these SOS relationships have not theoretically and experimentally reported yet.

Permutable SOS of $\mathscr{C} \cdot \mathscr{P}' \approx \boldsymbol{\alpha}'$, $\boldsymbol{\alpha} \cdot \boldsymbol{\alpha}' \approx \mathscr{D}'$, and $\mathscr{P} \cdot \mathscr{D}' \approx \mathscr{P}'$

We have also the dot product-type, rather than cross product-type, SOS relationships of $\mathscr{C} \cdot \mathscr{P}' \approx \boldsymbol{\alpha}'$, $\boldsymbol{\alpha} \cdot \boldsymbol{\alpha}' \approx \mathscr{D}'$, and $\mathscr{P} \cdot \mathscr{D}' \approx \mathscr{P}'$, as well as their permutable SOS relationships, summarized below: The broken symmetry operations that do not cancel on the left-hand side are colored in green as the resultant broken symmetries on the right-hand side, while canceled ones are colored in dark gray. Note that a dot product between two 1D objects means the coexistence of two 1D objects, and when a symmetry is broken in both 1D objects that are coupled to each other and act as a new 1D object, the symmetry can be not broken in the 3rd 1D object. For this situation, we have the following SOS relationships.

(1) $\mathscr{C} \bullet \mathscr{P}'$ ≈ Broken {**I**,**M**,<u>**M**</u>} ⊗ Broken {**R**,**I**,**M**,**T**} = Broken {**R**,<u>**M**</u>,**T**} ≈ $\boldsymbol{\alpha}'$

(2) $\mathscr{C}' \bullet \mathscr{P}$ ≈ Broken {**I**,**M**,<u>**M**</u>,**T**} ⊗ Broken {**R**,**I**,**M**} = Broken {**R**,<u>**M**</u>,**T**} ≈ $\boldsymbol{\alpha}'$

(3) $\mathscr{C}' \bullet \mathscr{P}'$ ≈ Broken {**I**,**M**,<u>**M**</u>,**T**} ⊗ Broken {**R**,**I**,**M**,**T**} = Broken {**R**,<u>**M**</u>} ≈ $\boldsymbol{\alpha}$

(4) $\boldsymbol{\alpha} \bullet \mathscr{C}'$ ≈ Broken {**R**,<u>**M**</u>} ⊗ Broken {**I**,**M**,<u>**M**</u>,**T**} = Broken {**R**,**I**,**M**,**T**} ≈ $\mathscr{P}'$

(5) $\boldsymbol{\alpha}' \bullet \mathscr{C}'$ ≈ Broken {**R**,<u>**M**</u>,**T**} ⊗ Broken {**I**,**M**,<u>**M**</u>,**T**} = Broken {**R**,**I**,**M**} ≈ $\mathscr{P}$

(6) $\boldsymbol{\alpha}' \bullet \mathscr{C}$ ≈ Broken {**R**,<u>**M**</u>,**T**} ⊗ Broken {**I**,**M**,<u>**M**</u>} = Broken {**R**,**I**,**M**,**T**} ≈ $\mathscr{P}'$

(7) $\mathscr{P} \bullet \boldsymbol{\alpha}'$ ≈ Broken {**R**,**I**,**M**} ⊗ Broken {**R**,<u>**M**</u>,**T**} = Broken {**I**,**M**,<u>**M**</u>,**T**} ≈ $\mathscr{C}'$

(8) $\mathscr{P}' \bullet \boldsymbol{\alpha}$ ≈ Broken {**R**,**I**,**M**,**T**} ⊗ Broken {**R**,<u>**M**</u>} = Broken {**I**,**M**,<u>**M**</u>,**T**} ≈ $\mathscr{C}'$

(9) $\mathscr{P}' \bullet \boldsymbol{\alpha}'$ ≈ Broken {**R**,**I**,**M**,**T**} ⊗ Broken {**R**,<u>**M**</u>,**T**} = Broken {**I**,**M**,<u>**M**</u>} ≈ $\mathscr{C}$

(10) $\mathscr{P} \bullet \boldsymbol{\alpha}$ ≈ Broken {**R**,**I**,**M**} ⊗ Broken {**R**,<u>**M**</u>} = Broken {**I**,**M**,<u>**M**</u>} ≈ $\mathscr{C}$

(11) $\boldsymbol{\alpha} \bullet \boldsymbol{\alpha}'$ ≈ Broken {**R**,<u>**M**</u>} ⊗ Broken {**R**,<u>**M**</u>,**T**} = Broken {**T**} ≈ $\mathscr{D}'$

(12) $\mathscr{P} \bullet \mathscr{D}'$ ≈ Broken {**R**,**I**,**M**} ⊗ Broken {**T**} = Broken {**R**,**I**,**M**,**T**} ≈ $\mathscr{P}'$

Note that $\mathscr{C}$, $\mathscr{C}'$, $\mathscr{D}$, and $\mathscr{D}'$ are director-like (i.e., not-broken {**R**}), so the resulting SOS orientation is fixed by vector-like objects of $\mathscr{P}$, $\boldsymbol{\alpha}$, $\mathscr{P}'$, or $\boldsymbol{\alpha}'$. Thus, the directions of $\mathscr{C}$, $\mathscr{D}'$, and $\mathscr{C}'$ in Fig. 5 can be in the vertical, horizontal, or out-of-plane direction. (1)–(9) list all SOS relationships permutable from $\mathscr{C} \cdot \mathscr{P}' \approx \boldsymbol{\alpha}'$: each SOS relationship has two [']s. Similar sets of permutable SOS relationships are possible from (10) to (12). First, Fig. 2c/d, reproduced in Fig. 5a, and Fig. 2h/i correspond to (2) and (12), respectively. When **E** and **M** in Fig. 2c/d are replaced by **H** and **P**, respectively, it corresponds to (5). This demonstrates a permutable SOS relationship as well as the permutable (and duality) nature of linear magnetoelectric effects. Note also that (2) and (6) mean that all diagonal linear magnetoelectrics belongs to $\mathscr{C}'$ and any specimen constituents having SOS with $\mathscr{C}'$ exhibit diagonal linear magneto-electric effects. Table 1 lists the complete set of dot product-type SOS relationships among eight kinds of 1D objects (vector- or director-like quantities).

Permutable SOS relationships of (2), (5), and (7) can be also well exemplified in hexagonal rare-earth ferrites[22]. The A_2 phase of the system carries **P** ($\mathscr{P}$) along the c axis and in-plane magnetic monopole ($\mathscr{C}'$), and a net magnetic moment **M** ($\boldsymbol{\alpha}'$) along the c axis is, indeed, observed experimentally, which is neatly consistent with (2). Through a spin reorientation transition, the magnetic state transforms into the A_1 phase with magnetic toroidal moments ($\mathscr{P}'$),
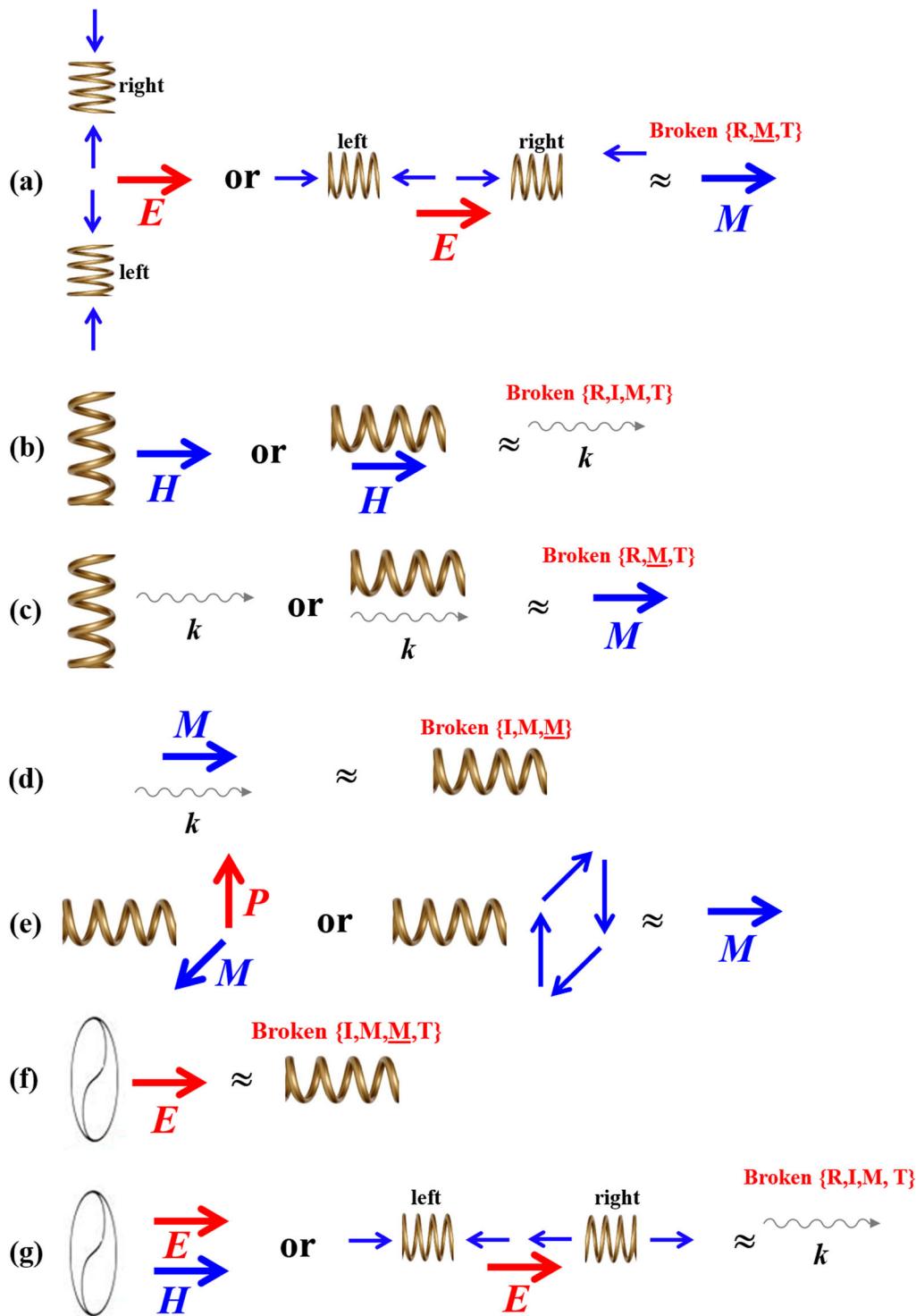
Fig. 5 Various SOS relationships. The Yin-yang symbol represents ferro-rotation. **a–g** correspond to $\mathscr{C}' \cdot \mathscr{P} \approx \alpha'$, $\alpha' \cdot \mathscr{C} \approx \mathscr{P}'$, $\mathscr{C} \cdot \mathscr{P}' \approx \alpha'$, $\mathscr{P}' \cdot \alpha' \approx \mathscr{C}$, $\mathscr{C} \cdot \mathscr{P} \approx \alpha'$, $\mathscr{P} \cdot \alpha \approx \mathscr{C}$, and $\alpha' \cdot \mathscr{C} \approx \mathscr{P} \cdot \mathscr{D}' \approx \mathscr{P}'$, respectively.

where the net magnetic moment M (α') is no longer allowed according to $\mathscr{P} \cdot \mathscr{P}' \approx \mathscr{D}'$. This is another premium example of how these permutable SOS relationships can be used to explain and predict physical properties in real materials.

Figure 5b corresponds to (6), which explains longitudinal and also transverse magnetochiral effects, i.e., non-reciprocal electronic transport or optical effects in chiral materials in the presence of external magnetic fields[23]. Note that a twisted graphene bilayer is

chiral, so exhibits a natural optical activity[24], and should exhibit non-reciprocal optical and also transport effects in the presence of magnetic fields, which need to be experimentally verified. Their inverse effects in Fig. 5c, corresponding to (1), include magnetization induced by electric current in chiral materials and spin-polarized tunneling in chiral materials. The magnetization induced by electric current in chiral Te single crystals has been reported in a Faraday-type optical experiment as well as a direct magnetization

pulse measurement[25,26]. The chirality-dependent spin-polarization of tunneling current was recently observed in chiral $Co_{1/3}NbS_2$[27] (see below). The existence of electric current in a magnetic field along the electric current direction corresponds to (9), so it corresponds to a chiral object (see Fig. 5d). In fact, this SOS relationship is closely related to the so-called chiral anomaly in topological Weyl semimetals, which are often non-chiral crystallographically[28–31]. Since the toroidal moment, just like $\boldsymbol{k}$, also belongs to $\mathscr{P}'$, the SOS in Fig. 5e should also work.

Chiral materials can exhibit natural optical activity, i.e., the rotation of light polarization of transmitted linearly-polarized light. Thus, Fig. 5f SOS relationship, corresponding to (10), explains the so-called linear-gyration, i.e., the linear change of the light polarization rotation of transmitted linearly-polarized light with the varying electric field. In fact, this linear-gyration can be utilized to visualize ferro-rotational domains, since opposite ferro-rotational domains show the opposite linear-gyration effects[1]. This idea was, indeed, confirmed in the visualization of ferro-rotational domains in ilmenite $NiTiO_3$, as shown in Fig. 6b[32]. There exists a large number of ferro-rotational compounds with point group symmetry of $\bar{1}, 2/m, \bar{3}, \bar{4}, 4/m, \bar{6}$ or $6/m$[33]. Examples include $Cu_3Nb_2O_8$ ($P\bar{1}$)[33],

$RbFe(MoO_4)_2$ ($P\bar{3}$ below 190 K)[34], $CaMn_7O_{12}$ ($R\bar{3}$ below 440 K)[35], NbO_2 ($I4_1/a$ below 1081 K)[36], and Pb_2CoTeO_6 ($R\bar{3}$ below 370 K)[37]. Ferro-rotational domain visualization of these compounds needs to be further investigated with the linear-gyration technique.

Figure 6a exhibits the atomic model of a topological vortex surrounded by six structural chiral domain boundaries in $Co_{1/3}NbS_2$. Since Co intercalants occupy one of three possible Nb-atop sites, A, B, and C, there exist six possible combinations considering the two layers within a unit cell, exhibiting A/B-type stacking. Solid and dashed lines refer to structural chiral domain boundaries in the first and the second layer, respectively. As a result of intercalation site change, the chiral distortion of the S layer reverses as depicted by red and blue triangular arrows and gives the alternating structural chirality across the vortex domain boundaries. In reference to the SOS relationship shown in Fig. 5c, flowing electric current across the chiral structure induces a magnetization along the current direction, which should work even for local probes such as scanning tunneling microscopy (STM). Figure 6b shows the spin-polarized STM (SP-STM) measurement around a topological vortex that clearly reveals the alternating domain contrast locked to the chirality of each domain[27]. It is noteworthy that the induced domain contrast does not require long-range ordered magnetic moments, in contrast to the conventional SP-STM. Instead, the specimen constituent comprised of the chiral structure and the tunneling current gives the same set of broken symmetries as magnetization, as shown in Fig. 5c.

We would like to note finally that ferro-rotation is rather common in numerous materials[33–37], but does not break inversion symmetry, so difficult to be coupled with measuring probes and thus has been studied only to a limited degree. The traditional way to study ferro-rotational domains is atomic-resolved transmission electron microscopy (TEM) such as high-resolution TEM or high-angle annular dark-field (HAADF)-STEM to observe the ferro-rotational distortions or ferro-rotational domains[32]. Figure 6e depicts a pair of ferro-rotational domains, corresponding to a clockwise and counterclockwise rotation of the FeO_6 octahedra in $RbFe(MoO_4)_2$. Utilizing the cryogenic dark-field TEM technique (Fig. 6f), the contrast difference between the two ferro-rotational domains shows up as the brighter

Table 1. Dot product-type SOS relationships among eight kinds of 1D objects (vector- or director-like quantities).

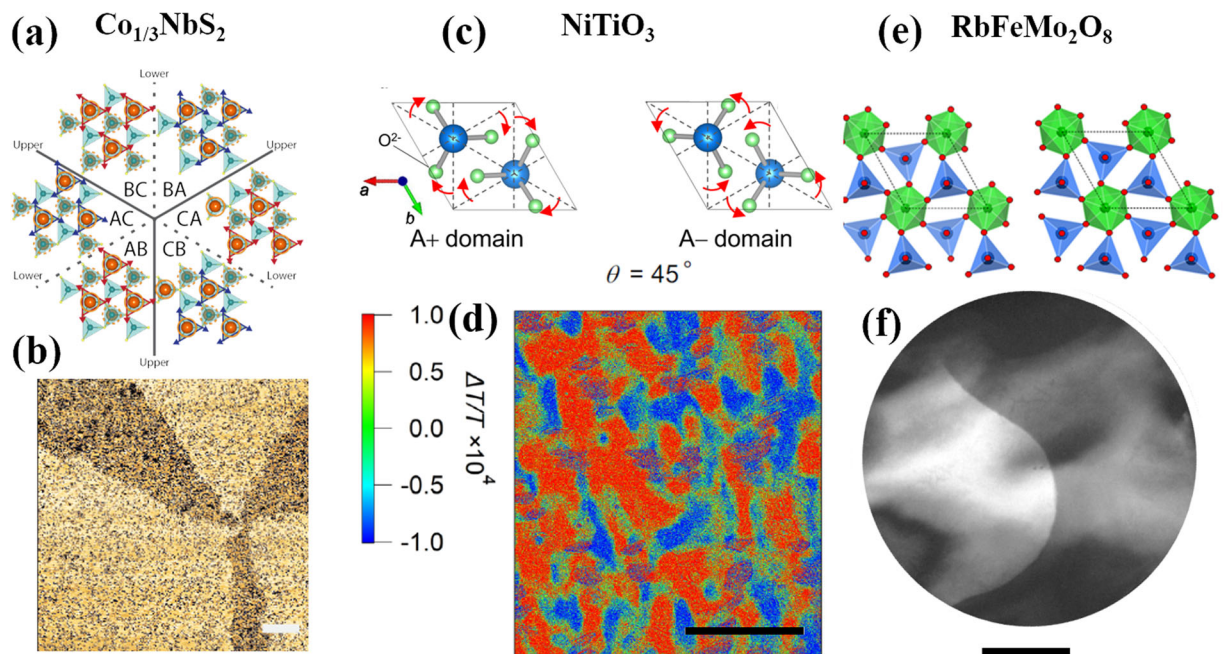|	$\mathscr{D}$	$\mathscr{C}$	$\mathscr{P}$	$\boldsymbol{a}$	$\mathscr{D}'$	$\mathscr{C}'$	$\mathscr{P}'$	$\boldsymbol{a}'$
$\mathscr{D}$	$\mathscr{D}$	$\mathscr{C}$	$\mathscr{P}$	$\boldsymbol{a}$	$\mathscr{D}'$	$\mathscr{C}'$	$\mathscr{P}'$	$\boldsymbol{a}'$
$\mathscr{C}$	$\mathscr{C}$	$\mathscr{D}$	$\boldsymbol{a}$	$\mathscr{P}$	$\mathscr{C}'$	$\mathscr{D}'$	$\boldsymbol{a}'$	$\mathscr{P}'$
$\mathscr{P}$	$\mathscr{P}$	$\boldsymbol{a}$	$\mathscr{D}$	$\mathscr{C}$	$\mathscr{P}'$	$\boldsymbol{a}'$	$\mathscr{D}'$	$\mathscr{C}'$
$\boldsymbol{a}$	$\boldsymbol{a}$	$\mathscr{P}$	$\mathscr{C}$	$\mathscr{D}$	$\boldsymbol{a}'$	$\mathscr{P}'$	$\mathscr{C}'$	$\mathscr{D}'$
$\mathscr{D}'$	$\mathscr{D}'$	$\mathscr{C}'$	$\mathscr{P}'$	$\boldsymbol{a}'$	$\mathscr{D}$	$\mathscr{C}$	$\mathscr{P}$	$\boldsymbol{a}$
$\mathscr{C}'$	$\mathscr{C}'$	$\mathscr{D}'$	$\boldsymbol{a}'$	$\mathscr{P}'$	$\mathscr{C}$	$\mathscr{D}$	$\boldsymbol{a}$	$\mathscr{P}$
$\mathscr{P}'$	$\mathscr{P}'$	$\boldsymbol{a}'$	$\mathscr{D}'$	$\mathscr{C}'$	$\mathscr{P}$	$\boldsymbol{a}$	$\mathscr{D}$	$\mathscr{C}$
$\boldsymbol{a}'$	$\boldsymbol{a}'$	$\mathscr{P}'$	$\mathscr{C}'$	$\mathscr{D}'$	$\boldsymbol{a}$	$\mathscr{P}$	$\mathscr{C}$	$\mathscr{D}$

Fig. 6 Visualization of domains associated with various broken symmetries. a A Z_6 vortex of $Co_{1/3}NbS_2$ with chiral domains. **b** Chirality-dependent SP-STM unveils a Z_6 vortex[27]. (scale bar = 20 nm). **c** The atomic structure of ferro-rotational domains of $NiTiO_3$[32]. **d** Ferro-rotational domains in $NiTiO_3$ visualized with an electro-gyration technique. (scale bar = 100 μm). **e** The atomic structure of ferro-rotational domains of $RbFe(MoO_4)_2$. **f** Ferro-rotational domains observed in TEM on $RbFe(MoO_4)_2$[38] (scale bar = 500 nm).

G_a spot for the left domain and the darker G_b spot for the right domain are collected. Note that the Bragg spot G_a is converted into G_b in the reciprocal space by the twofold rotation as two ferro-rotation domains do in real space[38]. The SOS relations of ferro-rotation such as Fig. 5f, g can be good guidance for the further exploration of ferro-rotations in the future.

In summary, the recent exotic experimental results such as electric current-induced magnetization in strained monolayer MoS_2, NLHE in monolayer WTe_2, spin-polarized tunneling in chiral $Co_{1/3}NbS_2$ in a paramagnetic state, and non-reciprocal electronic transport in polar BiTeBr can be understood in terms of permutable SOS relationships of 1D objects. We have presented all possible permutable SOS relationships among eight kinds of 1D objects. Based on the permutable SOS relationship, we have proposed a large number of new phenomena, which can be experimentally verified in the future. New predictions include (but are not limited to): (1) a twisted graphene bilayer in the presence of magnetic fields should exhibit non-reciprocal transport and optical effects [Note 1][39], (2) NLHE in strained monolayer MoS_2, (3) electric current-induced magnetization in monolayer Mo(W)Te_2, (4) electric current-induced magnetization, NLHE, and non-reciprocal electronic transport in bulk polar conductors such as $Ca_3Ru_2O_7$, GeTe, TaAs, and BiTeI(Br, Cl), (5) light- or thermal current-induced magnetization in numerous polar materials, (6) electric/thermal current-, or light-induced magnetization of polar materials at polar domain walls, (7) CDHE in any materials with enough electric conduction, (8) Ettingshausen, Nernst, or thermal Hall effect versions of CDHE in any materials with circularly-polarized light (or vortex beam with orbital angular momentum) illumination without any applied magnetic field, (9) non-reciprocal spin wave propagation in polar materials such as Fe(Mn,Ni,Zn)$_2Mo_3O_8$ or Ni_3TeO_6 in magnetic fields, (10) non-reciprocal directional dichroism in α-Fe_2O_3 below the Morin transition in the presence of an electric field, (11) visualization of ferro-rotational domains of ferro-rotational compounds such as RbFe(MoO$_4$)$_2$, $CaMn_7O_{12}$, $Cu_3Nb_2O_8$, NbO_2, and Pb_2CoTeO_6 using a linear-gyration technique, (12) non-reciprocal directional dichroism of electric current, spin wave or light in ferro-rotational systems in the presence of both electric and magnetic fields, and (13) the tiled induced polarization (current) and magnetization in ferro-rotational systems in the presence of an external electric field and magnetic field, respectively. We also find this important systematics: all magnetic states having SOS with $\mathscr{C}'$ exhibit diagonal linear magnetoelectric effects, and all magnetic states having SOS with $\mathscr{P}'$ exhibit off-diagonal linear magnetoelectric effects. It will be exuberating to confirm these predictions in bulk quantum materials as well as 2D materials in the coming years. The following poem summaries our findings in an esthetic manner:

Symmetry defines evident beauty.
Once broken, it brings observables.
Unveiling duality and permutability.
These tricks that Nature plays become the crystal ball to see its hidden beauty.
In Nature, nothing is perfect, yet everything is perfect. [Note 2]

Note 1: After submission of our manuscript, the following paper[39], directly relevant to this prediction, has published.

Note 2: Walker A. In nature, nothing is perfect and everything is perfect. Trees can be contorted, bent in weird ways, and they're still beautiful.

METHODS
SOS analysis
The relationships between quasi-1D specimen constituents (lattice distortions or spin arrangements in external magnetic field, electric fields or stress, and also their time evolution) and measuring probes/quantities (observables such as transmitting electrons, phonons, magnons, photons in various polarization states, including electrons or photons with spin or orbital angular momentum, bulk magnetization or polarization, and also experimental setups to measure, e.g., Hall-type effects) are examined in terms of their characteristics under various symmetry operations of rotation, space inversion, mirror reflection, and time reversal. When quasi-1D specimen constituents have identical or more (but not less) broken symmetries, compared with measuring probes/quantities, except translation symmetry and rotation symmetry around the 1D direction, they are said to exhibit SOS, and the corresponding phenomena can take place. In terms of SOS, we have considered the specimen constituents for light- or current-induced magnetization, NLHE, the spin polarization of electric current in non-magnetic or paramagnetic states, linear magneto-electric effects, and natural optical activity or non-reciprocal effects in the presence of an electric field. In addition, we have also discussed what new phenomena can be observed in ferro-rotational systems from SOS considerations.

DATA AVAILABILITY

REFERENCES
1. Cheong, S.-W. SOS: symmetry operational similarity. *npj Quant. Mater.* **4**, 53 (2019).
2. Cheong, S.-W. Trompe L'oeil ferromagnetism. *npj Quant. Mater.* **5**, 37 (2020).
3. Cheong, S.-W., Talbayev, D., Kiryukhin, V. & Saxena, A. Broken symmetries, non-reciprocity, and multiferroicity. *npj Quant. Mater.* **3**, 19 (2018).
4. Hlinka, J. Eight types of symmetrically distinct vectorlike physical quantities. *Phys. Rev. Lett.* **113**, 165502 (2014).
5. Popov, Y. F., Kadomtseva, A. M., Belov, D. V. & Vorob'ev, G. P. Magnetic-field-induced toroidal moment in the magnetoelectric Cr_2O_3. *JETP Lett.* **69**, 330–335 (1999).
6. Krichevtsov, B. B., Pavlov, V. V., Pisarev, R. V. & Gridnev, V. N. Spontaneous non-reciprocal reflection of light from antiferromagnetic Cr_2O_3. *J. Phys. Condens. Matter* **5**, 8233–8244 (1993).
7. Yu, S. et al. High-temperature terahertz optical diode effect without magnetic order in polar $FeZnMo_3O_8$. *Phys. Rev. Lett.* **120**, 037601 (2018).
8. Ideue, T. et al. Bulk rectification effect in a polar semiconductor. *Nat. Phys.* **13**, 578–583 (2017).
9. Yokosuk, M. et al. Nonreciprocal directional dichroism of a chiral magnet in the visible range. *npj Quant. Mater.* **5**, 20 (2020).
10. Ma, Q. et al. Observation of the nonlinear Hall effect under time-reversal-symmetric conditions. *Nature* **565**, 337–342 (2019).
11. Lee, J., Wang, Z., Xie, H., Mak, K. F. & Shan, J. Valley magnetoelectricity in single-layer MoS_2. *Nat. Mat.* **16**, 887–891 (2017).
12. Son, J., Kim, K.-H., Ahn, Y. H., Lee, H.-W. & Lee, J. Strain engineering of the Berry curvature dipole and valley magnetization in monolayer MoS_2. *Phys. Rev. Lett.* **123**, 036806 (2019).
13. Yoshida, Y. et al. Crystal and magnetic structure of $Ca_3Ru_2O_7$. *Phys. Rev. B* **72**, 054412 (2005).
14. Rabe, K. M. & Joannopoulos, J. D. Theory of the structural phase transition of GeTe. *Phys. Rev. B* **36**, 6631 (1987).
15. Liang, W. et al. Giant anisotropic nonlinear optical response in transition metal monopnictide Weyl semimetals. *Nat. Phys.* **13**, 350–355 (2017).
16. Ishizaka, K. et al. Giant Rashba-type spin splitting in bulk BiTeI. *Nat. Mater.* **10**, 521–526 (2011).
17. Qiong, M. et al. Observation of the nonlinear Hall effect under time-reversal-symmetric conditions. *Nat. Mater.* **565**, 337–342 (2019).
18. Zhou, Y. & Liu, F. Realization of an antiferromagnetic superatomic graphene: Dirac Mott insulator and circular dichroism Hall effect. *Nano Lett.* **21**, 230–235 (2021).
19. Ivchenko, E. L. & Pikus, G. E. New photogalvanic effect in gyrotropic crystals (Pis'ma Zh. Eksp. Teor. Fiz. 27, 640 (1978)). *JETP Lett.* **27**, 604–608 (1978).
20. Belinicher, V. I. Space-oscillating photocurrent in crystals without symmetry center. *Phys. Lett. A* **66**, 213–214 (1978).
21. Asnin, V. M. et al. Observation of a photo-emf that depend on the sign of the circular polarization of the light. (Pis'ma Zh. Eksp. Teor. Fiz. 28, 80–84 (1978)). *JETP Lett.* **28**, 74–77 (1978).

22. Du, K. et al. Vortex ferroelectric domains, large-loop weak ferromagnetic domains, and their decoupling in hexagonal (Lu, Sc)FeO$_3$. npj Quant. Mater. **3**, 33 (2018).
23. Nakagawa, N. et al. Magneto-chiral dichroism of CsCuCl$_3$. Phys. Rev. B **96**, 121102 (R) (2017).
24. Kim, C. J. et al. Chiral atomically thin films. Nat. Nanotechnol. **11**, 520–524 (2016).
25. Vorobev, L. E. et al. Optical-activity in tellurium induced by a current. JETP Lett. **29**, 441–445 (1979).
26. Furukawa, T., Shimokawa, Y., Kobayashi, K. & Itou, T. Observation of current induced bulk magnetization in elemental tellurium. Nat. Commun. **8**, 954 (2017).
27. Lim, S. J., Huang, F.-T., Pan, S., Wang, K. F., Kim, J.-W. & Cheong, S.-W. Magnetochiral spin-polarized tunneling in a paramagnetic state, Preprint at https://www.researchsquare.com/article/rs-70373/v1.
28. Zyuzin, A. A., Wu, S. & Burkov, A. A. Weyl semimetal with broken time reversal and inversion symmetries. Phys. Rev. B **85**, 165110 (2012).
29. Burkov, A. A. & Balents, L. Weyl semimetal in a topological insulator multilayer. Phys. Rev. Lett. **107**, 127205 (2011).
30. Bell, J. S. & Jackiw, R. A PCAC puzzle: π0→γγ in the σ-model. Nuovo Cim. A **60**, 47–61 (1969).
31. Adler, S. L. Axial-vector vertex in spinor electrodynamics. Phys. Rev. **177**, 2426–2438 (1969).
32. Hayashida, T. et al. Visualization of ferroaxial domains in an order-disorder type ferroaxial crystal. Nat. Commun. **11**, 4582 (2020).
33. Johnson, R. D. et al. Cu$_3$Nb$_2$O$_8$: a multiferroic with chiral coupling to the crystal structure. Phys. Rev. Lett. **107**, 137205 (2011).
34. Jin, W. et al. Observation of a ferro-rotational order coupled with second-order nonlinear optical fields. Nat. Phys. **16**, 42–46 (2020).
35. Johnson, R. D. et al. Giant improper ferroelectricity in the ferroaxial magnet CaMn$_7$O$_{12}$. Phys. Rev. Lett. **108**, 067201 (2012).
36. Pynn, R., Axe, J. D. & Thomas, R. Structural distortions in the low-temperature phase of NbO$_2$. Phys. Rev. B **13**, 2965–2975 (1976).
37. Ivanov, S. A., Nordblad, P., Mathieu, R., Tellgren, R. & Ritterd, C. Structural and magnetic properties of the ordered perovskite Pb$_2$CoTeO$_6$. Dalton Trans. **39**, 11136–11148 (2010).
38. Huang, F.-T., Admasu, A. S., Han, M. G. & Cheong, S.-W. TEM on ferro-rotational domains in RbFeMo$_2$O$_8$. To be published.
39. Liu, Y., Holder, T. & Yan, B. Chirality-induced giant unidirectional magnetoresistance in twisted bilayer graphene. Innovation **2**, 100085 (2021).

AUTHOR CONTRIBUTIONS
S.W.C. conceived and supervised the project. All authors were involved in various symmetry analyses. S.L. and F.-T.H. wrote the STM and TEM parts, respectively, K.D. wrote some of the example parts and S.W.C. wrote the remaining part.

COMPETING INTERESTS
The authors declare no competing interests.

ADDITIONAL INFORMATION
Correspondence and requests for materials should be addressed to S.-W.C.

Reprints and permission information is available at http://www.nature.com/reprints

Publisher's note Springer Nature remains neutral with regard to jurisdictional claims in published maps and institutional affiliations.